Optical and Quantum Electronics **23** *(1991) 1105–1134*

Recent developments in laser resonator design

V. MAGNI, G. VALENTINI, S. DE SILVESTRI
Centro di Elettronica Quantistica e Strumentazione Elettronica del CNR, Istituto di Fisica del Politecnico, Piazza L. Da Vinci, 32, 20133 Milan, Italy

Received 18 January; revised and accepted 22 April 1991

The problems related to resonators suitable for generation of diffraction-limited beams of high power or energy, and a few of the most significant recent solutions, are reviewed. In particular, this paper is addressed to two promising resonator configurations developed mainly for Nd:YAG (yttrium aluminium garnet) lasers: dynamically stable resonators of minimum misalignment sensitivity for lasers with a strong thermal lensing in the active rod and unstable resonators with variable reflectivity output mirrors of super-Gaussian profile. For both cases experimental data and simple design guidelines are discussed.

1. Introduction

The generation of diffraction-limited (i.e. spatially coherent) beams of high power or energy, required in many scientific and industrial applications, is still an open and pressing problem for both solid-state and gas lasers, such as CO_2 lasers and excimers. To this purpose the resonator plays a crucial role. In fact, although laser materials of very large volumes are available, clear and simple design procedures for resonators suitable for sustaining a fundamental transverse mode of large cross sectional area that can satisfactorily fill and exploit the laser medium are still to be defined. Stable resonators operating on the fundamental TEM_{00} mode produce, as known, high quality diffraction-limited beams; however, the transverse mode dimensions and, as a consequence, the extracted energy from the gain medium are generally small. On the other hand, traditional unstable resonators can sustain fundamental modes of wide cross section, but the output beam quality and divergence are degraded by the typical dark hole and by intense diffraction fringes originated by the reflectivity discontinuity of the output mirror.

This paper is mainly aimed at reviewing two solutions for diffraction-limited beam generation that we have developed and applied to Nd:YAG (yttrium aluminium garnet) lasers in recent years. The first (Section 2) concerns dynamically stable resonators of minimum misalignment sensitivity for continuous wave (c.w.) or high repetition rate solid state TEM_{00} lasers with a strong thermal lensing in the active rod. The second solution (Section 3) concerns unstable resonators with variable reflectivity output mirrors of super-Gaussian profile, which have been applied to a pulsed high gain Nd:YAG laser. The proposed design solutions are, however, of general validity and can be applied to any solid state and high gain gas lasers.

0306-8919/91 $03.00 + .12

2. Stable resonators with thermal lens for TEM_{00} mode operation

Multimode laser beams with an average power up to the kilowatt level can presently be generated with Nd : YAG lasers. On the contrary, the output power is reduced to a few tens of watts when a stable resonator operating on the fundamental transverse mode (TEM_{00}) is used, mainly because of the small overlapping volume of the TEM_{00} mode with the active material. Large mode volumes can be obtained with unstable resonators, but the high losses proper of unstable resonators hinder their use with low gain lasers, such as c.w. solid state lasers. To increase the output power with stable resonators, a large volume TEM_{00} is required. However, if appropriate design criteria are not applied, the resonator modes and the output power become dramatically sensitive to small perturbations and to mirror misalignment. The problem is further complicated by the lens effect produced in the rod by pumping. In fact, the rod dioptric power can reach considerable values even at moderate lamp input power levels (e.g. about 4 to 5 m^{-1} in Nd : YAG lasers) and plays a fundamental role in determining the performances of c.w. or high repetition rate solid state lasers. Since besides the gain of the active material, all properties of the resonant modes also depend on the pumping rate, the design of resonators for large mode volume TEM_{00} turns out to be very complicated.

Great efforts have been made to design stable resonators that can counteract or compensate for the thermal focusing of the rod. Early solutions proposed compensation of thermal lens by a convex mirror [1] or by diverging lenses ground on the end faces of the rod [2–4] that exactly eliminate the focusing effect: this compensation is, however, effective only at a given value of the pump power. Variations of the thermal focal length are allowed in concave–convex resonators [5], but only if the thermal effects are very small. An important step forwards was made with the introduction of dynamically stable resonators [6, 7], which allow reliable TEM_{00} mode operation with the mode volume stabilized against variations of thermal focal length (i.e. of pump power). The concept of dynamic stability has also been applied to resonators with an intracavity telescope, which give the advantage of an easy adjustment for different pump powers [8–11]. More recently it has been demonstrated that in dynamically stable resonators the position of the laser rod plays an important role, and a fine optimization allows substantial improvement of the performances [12, 13]. As far as multimode operation is concerned, various detailed studies and experimental data on resonators with an internal variable lens have been published: the optimization of the beam quality, divergence and output power has been considered [14–16], as well as multirod stable and unstable resonators [17–20].

Besides the dynamic stability, the mechanical stability of the resonator, i.e. the sensitivity to the mirror misalignment, is a key factor for designing stable resonators with large mode volume, since dynamically stable resonators might be unreliable because of the alignment difficulties [21, 22]. The misalignment sensitivity has been analysed by several authors [23–26]. For solid state lasers a comprehensive analysis of general resonators with an internal focusing rod was carried out and design procedure for optimized dynamically stable resonators with minimum misalignment sensitivity have been devised [21, 27]. The successful application to c.w. Nd : YAG lasers demonstrated a significant improvement of output power and of misalignment sensitivity [28, 29]. The general analysis mentioned has also been extended to cover the case of crystals other than YAG with very large focusing power [30] and resonators containing arbitrary optical elements [31, 32]. On the basis of [32] it has been demonstrated [33] that, independently of the resonator configuration, the range of input power for which the resonator is stable is inversely proportional to the mode

volume and is a unique characteristic of the laser material. To obtain higher TEM_{00} output power and wider stability range than those of YAG, laser crystals with low thermal focusing are required. Indeed, among the latest developments in this field, one of the most interesting concerns the Nd : YLF (lithium yttrium fluoride) laser, which presents a very low thermal focusing. The experimental results obtained with resonators, optimized following the design criteria developed for YAG, seem to demonstrate that Nd : YLF is definitely superior to YAG for TEM_{00} mode operation [34–36].

In Section 2 we first present a unified analysis of resonators with an internal variable lens that represents the pumped rod. The topic is treated in the widest generality, including also the possibility of an arbitrary intracavity optical systems (such as telescopes): the optical stability of the resonator, the mode volume and the misalignment sensitivity are studied, mainly as a function of the pump power, i.e. of the rod focal length. The theoretical findings are supported and confirmed by experimental results. Then, on these bases, simple and readily applicable design criteria for large mode volume, dynamically stable, minimum misalignment sensitivity resonators are described and their successful application to an Nd : YAG laser is presented.

2.1. Preliminary remarks

A considerable amount of heat is generated in the laser rod, mainly due to the pump quantum efficiency being less than unity and to the waste of energy between pump bands and laser levels. The heat removed from the rod surface generates a radial thermal gradient which, in turn, produces the following effects that contribute to the thermal lensing of the rod: a temperature-induced variation of the refractive index, a strain-dependent variation of the refractive index and an end face curvature caused by thermal expansion [37–41]. If heat generation is uniform, the bulk of the rod acts as a lens-like medium because of the quadratic variation of the refractive index as a function of the radius, whereas the term due to end face curvature introduces a small positive lens effect [39]. We can thus write for the rod focal length

$$1/f = (k/\pi a^2)P_{in} \tag{1}$$

where P_{in} is the electric pump power entering the lamp, a is the rod radius and k is a constant depending on the opto-mechanical properties of the laser rod and on the pumping efficiency. Since the location of the rod principal planes is almost independent of the pump power [21, 39, 42], the rod can be treated as a thin lens, provided that the distances from other optical elements are measured with reference to the principal planes of the rod. Note that if the effect due to the end face curvature is neglected, the rod dioptric power, as expressed by Equation 1, is independent of the rod length; indeed, the contribution of the end face curvature to the total focal length is generally less than 6% [39, 41], so the coefficient k can be considered as independent of the rod length.

To allow a very general analysis of solid state laser resonators, only two elements have to be considered: the rod and the intracavity optics. In this paper we consider only systems with rotational symmetry around the optical axis. The results of our analysis can be extended to astigmatic systems by considering separately two orthogonal axes [43]. A generic optical system is described by the suitable ray transfer matrix, and any possible misalignment of some component is treated by using a 2×1 vector in addition to the usual 2×2 matrix appropriate for aligned systems [31, 44–47].

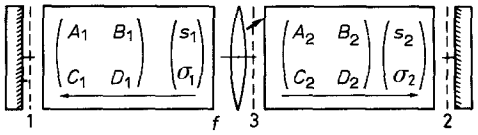

Figure 1 Linear resonator with an internal lens of variable focal length f and two generic intracavity optical systems. The arrows indicate that the matrices and the vectors represent the paths from the lens to the mirrors. The broken lines are reference planes.

For a generic optical system, assuming the optical axis as a reference, the position and the slope of the rays at the output plane (x_0, θ_0) are related to the corresponding quantities at the input plane (x_i, θ_i) by an equation that, as for perfect alignment, is linear, but no longer homogeneous

$$\begin{pmatrix} x_0 \\ \theta_0 \end{pmatrix} = \begin{pmatrix} A & B \\ C & D \end{pmatrix} \begin{pmatrix} x_i \\ \theta_i \end{pmatrix} + \begin{pmatrix} s \\ \sigma \end{pmatrix} \tag{2}$$

The elements of the misalignment vector (s, σ) give the position and the slope of the output ray when the input ray coincides with the reference axis of the system. The misalignment vector of a complex system is obtained by matrix multiplication [44, 47] on the basis of Equation 2. Because of linearity, the superposition principle can be used to evaluate the effect of the misalignment of each simple element composing a complex system. Thus, the misalignment vector is the sum of the output ray vectors obtained by assuming an input ray coincident with the reference axis and taking one misalignment at a time. In practice, s and σ result in a linear combination of tilting angle and displacements of the various decentred elements. To formulate the resonator properties in the widest generality we consider the resonator of a solid state laser modelled as shown in Fig. 1. It is composed of two plane mirrors that enclose a lens of variable focal length, f, (representing the rod) between two optical systems. The ray transfer matrices and the misalignment vectors shown in Fig. 1 are associated with the ray paths from the lens to the plane mirrors and include the possible mirror curvatures and misalignments. In fact, curved mirrors can be resolved in a plane mirror and a lens of focal length equal to the radius of curvature of the mirror.

2.2. Stability and mode volume

To make the equations that follow more readable, we define, with reference to Fig. 1, the variables

$$\eta = (1/f) - \tfrac{1}{2}[(A_1/B_1) + (C_1/D_1) + (A_2/B_2) + (C_2/D_2)] \tag{3}$$

$$u = (1/2B_1D_1) - 1/(2B_2D_2) \tag{4}$$

$$v = -(1/2B_1D_1) - 1/(2B_2D_2) \tag{5}$$

With this notation the transfer matrix T for propagation from mirror 1 to mirror 2 (see Fig. 1) is

$$T = -\begin{pmatrix} D_1B_2(\eta + u) & B_1B_2(\eta + v) \\ D_1D_2(\eta - v) & B_1D_2(\eta - u) \end{pmatrix} \tag{6}$$

Note that the only variable that depends on f, i.e. on the pump power, is η and that the matrix elements are linear functions of $1/f$.

The condition for the optical stability of the resonator $(0 < AD < 1)$ can also be expressed as [31, 48]

$$ABCD < 0 \tag{7}$$

TABLE I Stability limits of a resonator containing a variable lens

Stability limit	Value of η	Rod dioptric power	Stability zone	
			$uv > 0$	$uv < 0$
$A = 0$	$-u$	$\frac{C_1}{D_1} + \frac{A_2}{B_2}$	I	II
$D = 0$	u	$\frac{A_1}{B_1} + \frac{C_2}{D_2}$	II	I
$B = 0$	$-v$	$\frac{A_1}{B_1} + \frac{A_2}{B_2}$	I	II
$C = 0$	v	$\frac{C_1}{D_1} + \frac{C_2}{D_2}$	II	I

where A, B, C and D are the elements of the matrix T. Therefore, the stability limits as a function of η are obtained by equating to zero each element of the matrix T: from Equation 6 we immediately obtain $\eta = \pm u$ and $\eta = \pm v$. The corresponding expressions in terms of the rod dioptric power are listed in Table I. From Equations 6 and 7 we deduce that, as a function of the rod dioptric power, there are always two stability zones that are symmetrically located around the zero of the η axis and that have the same width $\Delta\eta$, given by

$$\begin{aligned} \Delta\eta = \Delta(1/f) &= \min(|u + v|, |u - v|) \\ &= \min(|1/B_1D_1|, |1/B_2D_2|) \end{aligned} \tag{8}$$

It is worth noting that the stability zones are crossed simply by varying the input power to the lamp. For a reason related to the misalignment sensitivity, which is discussed below, we denote by zone I the stability interval limited at one of the extremes by $\eta = -v$ (i.e. $B = 0$) and by zone II the interval limited by $\eta = v$ (i.e. $C = 0$). Note that v and $-v$ cannot be the boundary of the same zone. The second stability limit of each zone ($+u$ or $-u$) is immediately obtained by bearing in mind that in each zone η has a constant sign. Table I also indicates the zone corresponding to each limit both for $uv < 0$ and $uv > 0$.

The spot size (halfwidth $1/e^2$ of the intensity) w_3 of the TEM_{00} mode on the lens, calculated with the standard matrix method [31, 48, 49] by assuming that a Gaussian beam reproduces itself after one round trip, can be expressed as

$$w_3^4 = -(2\lambda/\pi)^2\eta^2/[(\eta^2 - u^2)(\eta^2 - v^2)] \tag{9}$$

where λ is the laser wavelength. The diagram of Equation 9 as a function of η, i.e. of the rod dioptric power $1/f$, is plotted in Fig. 2a. This plot shows that the spot size w_3 goes to infinity at the stability limits and reaches a minimum in each stablity zone. At this minimum the resonator is dynamically stable [6, 7, 21, 31], since the spot size in the rod is, to first order, insensitive to the variation of the focal length of the rod. Equating to zero the derivative of Equation 9 and solving for η, we obtain

$$\eta = \pm|uv|^{1/2} \tag{10}$$

The value w_{30} of the spot size w_3 for both of these values of η is

$$w_{30}^2 = (2\lambda/\pi)[1/\Delta(1/f)] \tag{11}$$

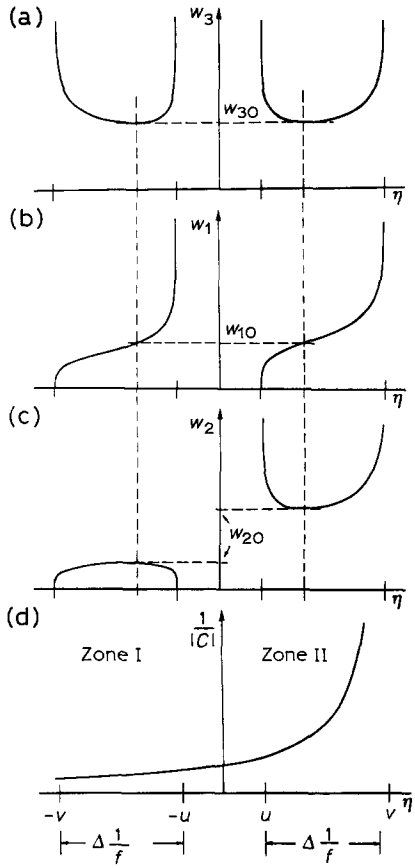

Figure 2 Spot sizes and misalignment sensitivity of the resonator with an internal variable lens of Fig. 1 for $uv > 0$ and $|u| < |v|$ as a function of η (dioptric power of the lens shifted by a constant amount). (a) Spot size on the lens, (b) spot size on mirror 1, (c) spot size on mirror 2, (d) absolute value of the focal length of the optics between mirrors (power of the mirrors included), which determines the misalignment sensitivity. The broken lines correspond to the dynamic stability.

where $\Delta(1/f)$ is given by Equation 8. This equation indicates that, independently of the resonator configuration, the volume of the TEM_{00} mode in the rod at dynamic stability is inversely proportional to the range of dioptric power for which the resonator is stable. The proportionality coefficient depends only on the laser wavelength.

The qualitative behaviour of the TEM_{00} mode spot sizes on the mirrors are also shown in Fig. 2b and c as a function of η, assuming that $|u| < |v|$. The picture for $|u| > |v|$ can be easily obtained with the help of Table I. Figure 2 shows that inside the stability zones the spot sizes have a quite smooth dependence on η, whereas they rapidly diverge or drop to zero as η approaches the stability limits. Therefore, the values of the spot sizes at dynamic stability can be considered to be representative of the mode dimensions in the whole stability zone; thus, Equation 11 can be conveniently used for a good approximate evaluation also if the resonator is not dynamically stable.

The existence and the characteristics of the stability zones have been investigated experimentally [27, 50] using an Nd : YAG laser with a rod 3 mm × 75 mm. The resonator was 1380 mm long and made by a convex mirror of − 1200 mm radius and a plane mirror with 10% transmission. This configuration was chosen as it allows the laser to operate in both zone I and zone II within the current range of the power supply. The TEM_{00} was selected by using suitable apertures. Figure 3 shows the laser output power as a function of the pump power for three difference distances of the rod from the convex mirror. The figure clearly

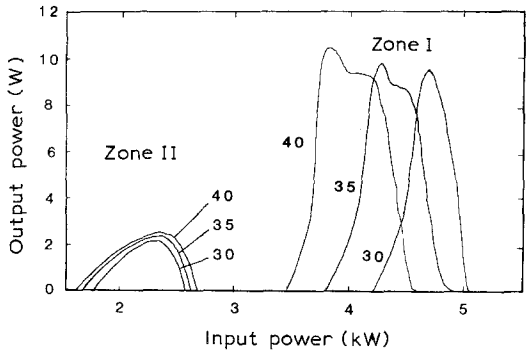

Figure 3 Experimental output power in fundamental mode operation of a c.w. Nd:YAG laser as a function of the electrical input power to the lamp for different positions of the rod. The resonator is 138 cm long, one mirror is flat and the other is convex (−120 cm radius). The parameter on the curve is the distance of the rod principal plane from the convex mirror.

shows the existence of two well-separated stability zones that are characterized by a second laser threshold at higher pump power besides the usual threshold at lower input power. All thresholds are determined by the large diffraction losses at the stability boundaries. As predicted by the theory, at the stability edges the spot sizes diverge rapidly; this behaviour explains the almost vertical drop of the output power at the stability limits. By varying the rod position inside the resonator, the input–output curves change their thresholds according to the relationship of Table I, which gives the rod dioptric power at the stability limits.

2.3. Pump power stability range

A more practical and interesting expression for the stability range is obtained by expressing the width of the stability zones in terms of the pump power [33]. Combining Equations 1 and 11 yields

$$\Delta P_{in} = (2\lambda/k)(a/w_{30})^2 \tag{12}$$

The quantity $(a/w_{30})^2$ is the ratio between the cross sections of the rod and the TEM_{00} mode. For an optimized resonator the mode cross section in the rod must be as large as possible for a full exploitation of the active medium. Therefore, for efficient TEM_{00} mode operation the rod must be the limiting aperture. Since it has been verified experimentally that for good TEM_{00} operation the ratio between the limiting aperture radius and the mode spot size should be allowed to vary between 1.2 and 2 [5, 7, 9, 26, 28, 51], the ratio a/w_{30} is approximately a constant and is independent of the rod size. It is clear from Equation 12 that, independently of the particular resonator configuration and rod dimensions, the input power range for which the resonator is stable (and for which the laser can operate) depends on only the parameter k. This quantity is related to the optomechanical properties of the laser medium and to the pump power conversions rate in heat, again related to the spectroscopic properties of the material and to the pumping efficiency. In general, the pump cavity is well optimized so that the pump power conversion rate in heat is established by the given material. It follows that ΔP_{in} can be assumed to be a figure of merit of the solid state laser material. As an example, assuming $a/w_{30} = 1.5$ to 1.8 and using the data reported in the literature for the dependence of the focal length on the pump power for Nd:YAG [39, 52] we calculate $\Delta P_{in} = 300$ to 500 W. For Nd:Cr:GSGG (gadolinium–scandium–gallium garnet), which has a much stronger thermal focusing [53, 54], we obtain $\Delta P_{in} = 50$ to 90 W. For Nd:YLF the situation is more favourable because of the very weak thermal focusing [34–36]: the stability range is 1.9 to 3.1 kW for π-polarized light and even greater than 6.5 kW for σ-polarized light. The stability range of Nd:YLF can be further increased

by cancellation of thermal lensing in a pair of suitably oriented rods [55]. The possibility of making athermal rods of Nd:BEL (lanthanum beryllate) by judicious selection of crystallographic orientation has also been explored [56]. Note that we have indicated a range of values for ΔP_{in} because of the spread of the data reported in the literature for the dependence of the focal length on the pump power, which is due mainly to the differences in the pumping efficiencies. We think, however, that the given values of ΔP_{in} are well representative of the real situation.

For a high average power laser, the small pump power stability range may represent a serious problem. To overcome it, three possible solutions may be envisaged: the use of athermal materials with low thermal focusing, the reduction of the unused radiation absorbed by the rod through optimization of the pump source, and the reduction of the spot size in the rod to enhance the ratio a/w_{30}. The first solution is certainly the most convenient in the case where athermal materials are available (for instance, some glasses or YLF). Optimization of pumping and reduction of dissipated heat can be obtained with diode pumping. Conversely, a reduction of the spot size in the rod is not really a good solution. In fact, for TEM_{00} operation the rod must be apertured, which results in a reduction of the output power and efficiency. An increment of the operating range by a factor of 2 can also be gained by designing the resonator with the two stability zones joined. It should be noted, however, that this procedure may lead to a resonator with an unacceptably high misalignment sensitivity: particular design precautions (as discussed below) must be considered in order to avoid the divergence of the misalignment sensitivity in the middle of the operating range.

2.4. Misalignment sensitivity

The additional power losses introduced by misalignment of a component of the resonator arise essentially from the displacement of the mode axis and of the transverse field pattern on the plane of the limiting (mode-selecting) aperture, which in solid state lasers having the mode that fully utilizes the active material is generally constituted by the rod cross section. The position and the axis of the resonator modes coincide with the ray that retraces itself after one round trip around the resonator [31, 44, 47], which, for a perfectly aligned resonator, obviously coincides with the optical axis of the system. If we denote by (x_3, θ_3) the position and the slope at the reference plane marked 3 in Fig. 1, the solution of the self-consistency equation, expressing the fact that a ray retraces itself after a round trip, gives [31]

$$\begin{pmatrix} x_3 \\ \theta_3 \end{pmatrix} = -\frac{1}{C}\begin{pmatrix} D_2\sigma_1 + D_1\sigma_2 \\ -C_2\sigma_1 + [C_1 - \Delta(D_1/f)]\sigma_2 \end{pmatrix} \tag{13}$$

where C is the (2, 1) element of the matrix given in Equation 6 and is the opposite of the dioptric power of the optics between the end mirrors (with the power of the mirrors included). The detailed expression for the position and the slope of the mode axis as a function of the tilting and displacement of each decentred element can obviously be calculated only when a particular configuration is specified. However, it can be shown that the effects of mirror misalignments are given directly by Equation 13, considering σ_1 and σ_2 as the tilting angles of the end mirrors. Equation 13 makes clear that, whichever resonator component is misaligned, the dependence of the axis displacement on the focal length of the rod is always contained only in the term $1/C$. The behaviour, as a function of η, of $|1/C|$ is also shown in Fig. 2d. From this figure it is apparent that one of the two

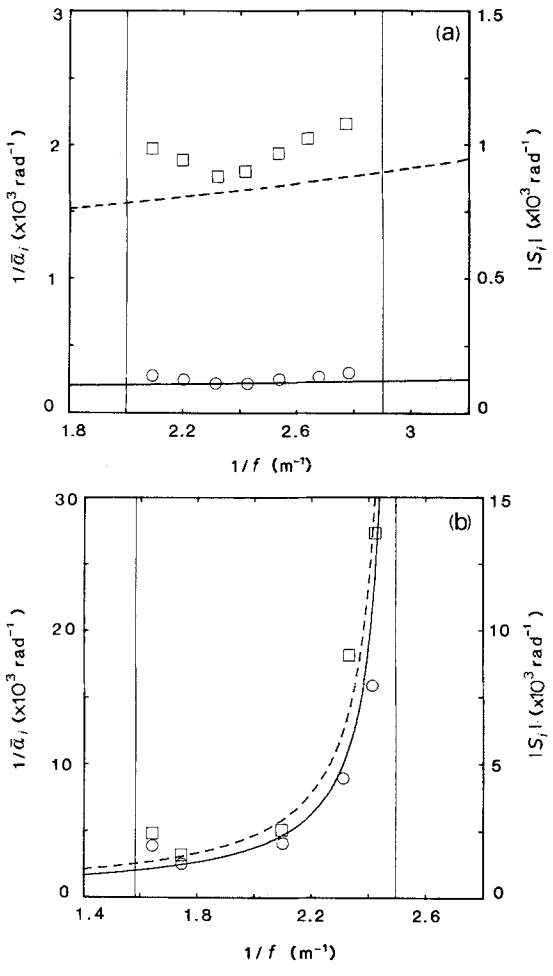

Figure 4 Theoretical misalignment sensitivity S_i (full and broken curves, right scale) and experimental values of the reciprocal of the half-power misalignment angle $1/\bar{\alpha}_i$ (○ and □, left scale) as a function of the rod dioptric power. The resonator is 153 cm long, the mirror radii are $R_1 = -120$ cm and $R_2 = 56$ cm. The distance of the rod from mirror 1 is 70 cm for zone I (a) and 27 cm for zone II (b). The point indicated as ○ (□) and the full (broken) curves refer to mirror 1 (2). The vertical lines delimit the stability range.

stability zones, denoted by zone II, is much more sensitive to misalignment than is the other, denoted by zone I. In particular, the diverging behaviour in zone II might be troublesome, especially when the stability range is small.

Considering a resonator made only by the rod and the two end mirrors, we can define two misalignment sensitivity factors as [21]

$$S_i = x_3(\alpha_i)/w_{30}\alpha_i \qquad i = 1, 2 \tag{14}$$

where α_i is the tilting angle of end mirror i that causes the mode axis to displace by $x_3(\alpha_i)$. Since the reduction of the output power as a consequence of misalignment is caused by the displacement of the mode away from the centre of the rod, assuming that the decrement by one-half is due to a given shifting of the mode axis, the reciprocal of the tilting angle that halves the output power can be considered to be proportional to the misalignment sensitivity factor given by Equation 14. Figure 4 represents, as an example, the experimental observation of the behaviour of the misalignment sensitivity factors [22, 29]. The full and broken curves are the calculated value of S_i and the experimental points are the reciprocals of the tilting angles $\bar{\alpha}_i$ of the end mirror that halve the output power of the laser. The measurements were

performed with two resonators differing only in the rod position, chosen to assure the same pump power level and the same stability range for both zone I (Fig. 3a) and zone II (Fig. 3b. It is remarkable that, apart from a proportionality factor taken into account by a suitable choice of the verticle scales, the theoretical misalignment sensitivity fits the experimental results quite well. Note also the markedly different sensitivity of the two zones and, in particular, the divergence of $1/\bar{\alpha}_i$, which closely follows that of S_i.

2.5. Design of optimized resonators

On the basis of the previously discussed results we now present the procedure for designing an optimized resonator [21]. We consider resonators made only by the focusing rod and the two end mirrors, since this approach provides for satisfactory solutions in most cases. Note, furthermore, that the addition of intracavity optics is not useful in increasing the mode volume when the pump power stability range (i.e. the width of the stability zone) is given. The resonator must be designed with consideration of the following requirements. First, a large mode volume in the rod is needed, so that the active material is exploited to the greatest extent, with the rod acting as the mode-selecting aperture. Secondly, dynamic stability is needed, so that the mode spot size in the rod is insensitive, to the first order, to fluctuations in the pump power. Finally, the misalignment sensitivity should be minimized, in order to maximize the mechanical stability of the resonator. The design procedure assumes three parameters of the laser as given, namely the rod diameter, the minimum rod focal length corresponding to the maximum pump power and the resonator length. The rod diameter determines the maximum value of the mode spot size in the rod, which must be sufficiently large to suppress oscillation of higher order modes without introducing too much loss for the TEM_{00}. Our experiments indicate 1.8 as an optimum value for the ratio between the rod radius and the TEM_{00} spot size, although slightly different values can be found in the literature [5, 7, 9, 26, 51]. The minimum rod focal length depends on the pump power level at which the laser is designed to operate, and is generally determined by the maximum thermal load sustained by the rod or by the power supply limits. Finally, the resonator length may be determined by the maximum dimensions acceptable for the laser or, in case of mode-locking operation, by the longitudinal-mode frequency separation needed. To determine the resonator configuration, which is sketched in Fig. 5, the radii of curvature of the mirrors (R_1 and R_2) and their distances from the principal planes of the rod (L_1 and L_2) need to be calculated. Following the previous considerations, we assume to know: (i) the spot size at dynamic stability, w_{30}, which is about 1.8 times less than the rod radius; (ii) the minimum focal length reached by the rod, f_{min}, which sets the maximum operating power level; (iii) the resonator equivalent length

$$L = L_1 + L_2 \tag{15}$$

Since L_1 and L_2 are the distances of the mirrors from the principal planes of the rod, L differs both from the physical distance between the mirrors and from the optical path

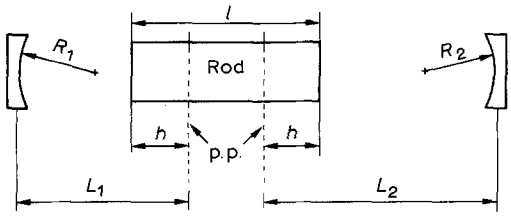

Figure 5 Resonator structure considered for the optimization. p.p., Principal plane of the rod, $h = l/2n$, n being the refractive index of the laser rod.

length [21]. The minimization of misalignment sensitivity immediately indicates that the laser must operate in zone I, so that $B = 0$ must be one of the two stability limits. With the help of Table I, by using the matrix elements appropriate to our case [57], this limit can be expressed as

$$1/L_1 + 1/L_2 = 1/f_B \tag{16}$$

where $1/f_B$ can be set equal to $1/f_{\min}$ or to $1/f_{\min} - \Delta(1/f)$, $\Delta(1/f)$ being given by Equation 11.

The spot size w_{30} is related to the resonator configuration through Equations 8 and 11. Without loss of generality we can assume that for our resonator $|B_1 D_1| > |B_2 D_2|$, since the opposite case would lead to the design of a symmetric configuration. From Equations 8 and 11 we thus have

$$w_{30}^2 = (2\lambda/\pi)|B_1 D_1| \tag{17}$$

which, by using the matrix element relevant to our case, can be written

$$w_{30}^2 = (2\lambda/\pi)L_1|1 - L_1/R_1| \tag{18}$$

Equations 15, 16 and 18 allow for the calculation of three of the four unknown resonator parameters, namely L_1, L_2 and R_1. However, four solutions may exist and, moreover, R_2 is still undetermined. To define the resonator precisely, the misalignment sensitivity, already controlled by the setting of the operating point in zone I, has to be optimized with the following considerations. Since the misalignment sensitivity, as given by Equation 14, is different for the two mirrors and is a function of the rod dioptric power $1/f$, we consider for safety the worst case. We first calculate the two maximum values of the misalignment sensitivity of the two mirrors $S_1(1/f)$ and $S_2(1/f)$, reached by varying $1/f$ within the stability zone; then we define the 'worst case' misalignment sensitivity, S_{wc}, as the higher of those two maxima. The quantity S_{wc} is a function of the distances L_1 and L_2 and of the mirror radii R_1 and R_2, but by definition does not depend on the rod power $1/f$:

$$S_{wc} = S_{wc}(R_1, R_2, L_1, L_2) \tag{19}$$

By solving Equations 15, 16 and 18 and by minimizing S_{wc}, we obtain the following expressions that define the resonator configuration:

$$L_1 = (L/2)[1 + (1 - 4f_{\min}/L)^{1/2}] \tag{20}$$

$$L_2 = L - L_1 \tag{21}$$

$$1/R_1 = (1/L_1)[1 - (\pi/2\lambda)(w_{30}^2/L_1)] \tag{22}$$

$$L_1/L_2R_1 \leqslant 1/R_2 \leqslant 1/L_2 \tag{23}$$

Note that the greater value of the rod dioptric power in the operating zone, $1/f_{\min}$, corresponds to the stability limit $B = 0$ (i.e. $f_B = f_{\min}$). Equation 20 shows that a real solution exists only if $L > 4f_{\min}$: this constraint is related to the fact that at the stability limit $B = 0$ the rod thermal lens images the two end mirrors on to each other, and this is possible only if the distance between source and image is at least four times the focal length of the lens. Note also that the radius R_2 can be freely chosen within the interval given by Equation 23 without affecting the stability limits, the spot size w_{30} or the value of S_{wc}. The last quantity is found to be $S_{wc} = L_2/w_{30}$ and corresponds to the misalignment sensitivity of mirror 2 at the stability limit $1/f = 1/f_{\min} - \Delta(1/f)$. Note, finally, that once the resonator

has been set up, a fine optimization of the laser performance is still experimentally possible (following [12]) by moving the laser rod and leaving the total resonator length and the mirror radii unchanged.

For a given w_{30} the stability range can be doubled if the resonator is designed so that the stability zones are joined; the price paid in this case is a higher misalignment sensitivity. With the help of Table I we can conclude that the two zones collapse in a wider zone if $v = 0$ or $u = 0$; in the former case, however, the stability limits $C = 0$ and $B = 0$ are reached for the same value of rod focal length and coincide with the centre of the overall stability range, so that the divergence of the misalignment sensitivity occurs exactly in the middle of the stability zone, which prevents any practical utilization of such a configuration. Therefore, it is preferable to set $u = 0$, so that the misalignment sensitivity diverges at one of the overall stability limits. The best configuration in this case is obtained with L_1, L_2 and R_1 again given by Equations 20 to 22. The radius R_2 is determined by

$$1/R_2 = (1/L_2[1 - (\pi/2\lambda)(w_{30}^2/L_2)] \tag{24}$$

Note that, also in this case, the stability limit $B = 0$ corresponds to the maximum pump power level of the stability zone. Moreover, note that the misalignment sensitivity diverges for a pump power corresponding to the lower limit of the overall stability zone (i.e. for $1/f = 1/f_{\min} - 2\Delta(1/f)$) and that in the centre of the overall stability range mirror 1 is the more sensitive, with $S_1 = L_1/w_{30}$.

The key features of the proposed design procedure that make it very simple and readily applicable can therefore be summarized as follows: the operating pump power level is essentially set only by the distances of the mirrors from the rod; the curvature of one mirror (R_1) together with the distance from the rod (L_1) determine the mode spot size in the rod; finally, the curvature of the second mirror (R_2) does not influence either the operating pump power level or the mode volume, but only sets the misalignment sensitivity. As an example of the application of this procedure, we consider the design of an Nd : YAG laser using a rod with a diameter of 3 mm and length of 75 mm, whose focal length is $f_{\min} = 257$ mm at 5.0 kW pump power. The resonator length is $L = 1351$ mm and the appropriate spot size is $w_{30} = 0.83$ mm. The optimized resonator satisfying these conditions, sketched in Fig. 6a, has $L_1 = 1006$ mm, $L_2 = 345$ mm and $R_1 = \infty$. For the radius of mirror 2, $R_2 = 400$ mm has been chosen, according to Equation 23. The output is taken from the plane mirror, which has a reflectivity of 80%. The output power as a function of the input power is shown as curve a in Fig. 6c. The maximum of the curve reaches about 18 W. This laser, when mode-locked with an acousto-optic modulator, gives an average output power of 14 W with pulses of 90 ps (full width at half-maximum, FWHM). The short pulse duration gives evidence of a very pure single transverse mode operation. The optimization of the misalignment sensitivity leads to a considerable mechanical stability: in fact, the tilting angle to reduce by 50% the output power at the peak of the curve is 1.1 mrad for the concave mirror and 10 mrad for the plane mirror. For the same laser under the same conditions, a resonator with the joined zones has also been tested. The configuration obtained is shown in Fig. 6b. Essentially, the concave mirror is replaced by a convex mirror of -190 mm radius, whereas the distances L_1 and L_2 are slightly different from those of the previous resonator to allow the utilization of the available radii of curvature for mirror 2. The output power curve is shown in Fig. 6c as curve b. It can be seen that in this case the maximum power is also about 18 W. The operation in the mode-locking regime gives the same results as in the previous case. Although the misalignment sensitivity is higher than before, it is still satisfactory; at

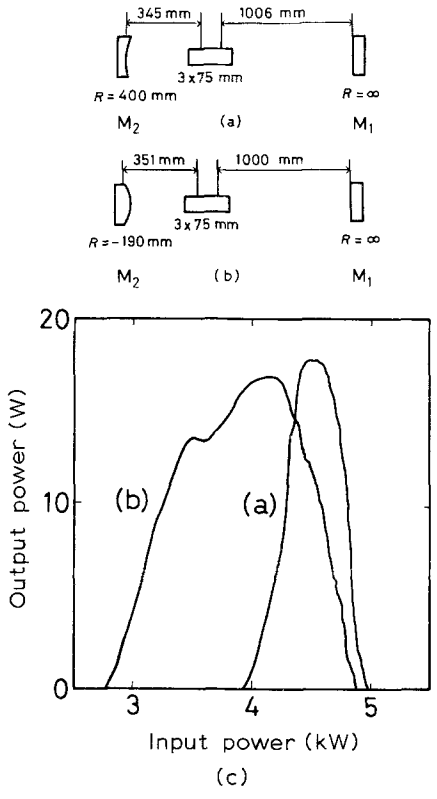

Figure 6 Output power in the single transverse fundamental mode as a function of the input power to the lamp for the optimized resonators shown on the top. The mirror distances are measured with reference to the rod principal planes located at 21 mm from the rod faces.

the peak of the output power curve the half-power angle for the convex mirror is 2.2 mrad and is 0.71 mrad for the plane mirror. A comparison of these results with data available from the literature and from technical data sheets confirms that the reported value of the output power (18 W) should be very close to the maximum obtainable from an Nd : YAG rod of the given size (3 mm × 75 mm).

As shown in Fig. 6, in practice, TEM_{00} Nd : YAG lasers of high power can work only at the value of input power corresponding to the peak of the output power curve. To overcome the limitation caused by the very small stability range of Nd : YAG, materials with lower thermal lensing (such as Nd : YLF) must be used. In recent years high quality Nd : YLF rods of suitable sizes have become available and very promising results have been demonstrated [34–36]: output powers in TEM_{00} mode as high as 35 W have been obtained with a rod of 4 mm diameter by 75 mm length [36]. In this case the resonator design essentially followed the guidelines applicable to the Nd : YAG laser; however, since the thermal focal length of YLF is typically greater than a few metres, a positive glass lens was inserted in the resonator to allow operation in zone I and reduction of misalignment sensitivity. In addition, Nd : YLF presents thermal astigmatism, which must be compensated by a cylindrical lens [34–36, 58].

3. Unstable resonators with variable-reflectivity mirrors

A usual technique to generate diffraction-limited laser beams of high power or energy relies on the use of unstable resonators. This solution is well suited especially to lasers having an

active medium of large cross section and high gain (such as pulsed Nd : YAG, excimer and CO_2 lasers) since the electromagnetic field provides a wide filling of the active material, allowing an efficient coupling between the optical mode and the gain medium. Besides this advantage, however, there are some drawbacks. In traditional unstable resonators the output beam is extracted around the edge of a totally reflecting mirror and presents a typical doughnut shape with highly pronounced fringes produced by the diffraction wavelets originating at the mirror edge. Furthermore, owing to the mode-crossing phenomenon [59, 60], the transverse mode discrimination may be critical and the resultant beam quality is significantly reduced compared with that of stable resonators operating in TEM_{00} mode. The low beam quality also affects the far-field profile, where a remarkable fraction of the energy is spread in side lobes around the central peak, worsening the divergence. To overcome these shortcomings, a number of new unstable resonator configurations have recently been proposed. Among these, the most significant are the self-filtering unstable resonator (SFUR) [61–63], the unstable resonators with a phase-unifying partially transmitting output coupler [64, 65] and the unstable resonators using a transmitting coupler with a radially variable reflectivity profile.

In the following we treat in detail the properties of unstable resonators with a variable-reflectivity mirror (VRM). By using these mirrors, the hole in the near-field disappears, leaving a dip whose depth and width depend on the resonator configurations, the diffraction fringes are greatly reduced, due to the absence of the mirror sharp edge, and the losses degeneracy is removed [66], giving greater transverse mode discrimination. As a consequence, the near-field is more uniform, with a significant reduction of the high frequency components, and the mode purity is increased; these effects are also reflected in the far-field, where the energy fraction present in side lobes around the central peak is greatly reduced.

3.1 Variable-reflectivity output couplers

Since the introduction of resonators with radially variable-reflectivity mirrors, various devices have been proposed and tested. The first device with radially variable-reflectivity profile that was implemented is the radial birefringent element (RBE) [67, 68]. This apparatus essentially consists of a birefringent crystal, ground to form a lens, and a polarizer inserted inside the resonator near one of the mirrors. When a linearly polarized wave impinges on the birefringent lens, its polarization is rotated by an angle that depends on the thickness of the material and hence on the distance from the lens axis. After traversing the lens, the beam goes through the polarizer, which transforms the variations of polarization into variations of intensity of the reflected (and transmitted) light. Generally, the polarizer is used as an output coupler. This device has been applied to a pulsed Nd : YAG laser [67] and to pulsed alexandrite and ruby lasers [69]. In each case, the superiority of unstable resonators with a variable-reflectivity coupler to standard unstable resonators in generating diffraction limited beam has been demonstrated. The components of an RBE can be easily fabricated, but this technique does not promise convenient applications to high power lasers, especially in the infrared region, where finding suitable birefringent materials and polarizers is difficult. Moreover, in solid state lasers the thermally induced birefringence in the rod may interfere with the operation of the RBE.

Another radially variable output coupler consists of two rectangular glass prisms almost in contact along the diagonal surfaces which, instead of being planar, are optically polished to a suitable curvature [70]. At the interface between the curved surfaces part of the light from the first prism is coupled into the second prism through evanescent waves; since the

separation between the surfaces depends on the distance from the centre, the transmitted intensity changes with that distance. The reflected wave, which is used to couple light out of the cavity, behaves in a complementary way. Up to now this device has been applied only to an excimer laser [70]. The critical positioning of the two prisms and their astigmatism seem to hinder the widespread practical application of this technique.

Another device proposed as a radially variable output coupler is the radially variable Fabry–Perot interferometer (RAVI) [71, 72]. The apparatus essentially consists of two mirrors of different radii of curvature facing each other with a small separation. The two facing surfaces are curved and coated to a suitable reflectivity, whereas the external surfaces are anti-reflection coated. The reflectivity profile, determined by the interference of the waves reflected by the two coated surfaces, is a function of the distance between the surfaces and therefore varies radially. The RAVI has been used in a pulsed Nd:YAG laser to produce diffraction-limited beams [72]. The main difficulty in using the RAVI lies on the critical positioning of the two mirrors of the interferometer.

Undoubtedly the most effective and promising technique for implementing radially variable reflectivity mirrors is based on the deposition of a shaped thin dielectric layer of high refractive index on an anti-reflection-coated transparent substrate. The reflectivity is determined by the multiple interference inside the shaped dielectric film, and therefore changes with the radial coordinate. In principle, the dielectric variable-reflectivity mirrors can be adapted in peak reflectivity, size and wavelength to any laser.

The first dielectric mirrors with Gaussian reflectivity profile have been realized for a wavelength of 10 μm, by depositing a variable-thickness layer of germanium on anti-reflection-coated substrates of germanium or sodium chloride [73]. Gaussian mirrors of this type were used in atmospheric pressure CO_2 lasers with a confocal unstable resonator to produce diffraction-limited beams without fringes in the near-field and side lobes in the far-field [74, 75]. The usefulness of Gaussian mirrors for the operation of CO_2 lasers in single transverse and longitudinal mode has also been demonstrated [76, 77].

More recently dielectric Gaussian mirrors for the wavelength 1.06 μm have been fabricated [78] and used [79] in a pulsed Nd:YAG from which diffraction-limited beams of smooth near- and far-field profiles, with energy of about 250 mJ (at 17 J input energy), have been obtained. Significant results were also obtained with a pulsed Nd:YAG laser by using a mirror with a parabolic reflectivity profile [80].

The availability of variable-reflectivity mirrors whose parameters (size, peak reflectivity and shape) can be tuned independently is extremely important in the practical realization of a number of different design specifications. The super-Gaussian mirrors (see Section 3.3), which have been recently introduced for Nd:YAG lasers [81, 82], besides allowing large mode volume, can also satisfy this requirement. To this purpose, a thin-film vacuum deposition technique has been developed which allows the fabrication of multidielectric mirrors whose reflectivity profile is entirely under control. This method is essentially based on the shadowing effect of a fixed non-contact mask with a circular aperture, placed between the crucible and the substrate [83]. As an example, the reflectivity profiles of four super-Gaussian mirrors fabricated with this technique are shown in Fig. 7. The mirrors consist of a glass substrate covered with a double-layer anti-reflection coating over which a third layer of high refractive index material has been deposited. The thickness of the upper layer is radially decreasing from about $\lambda/4$ to zero, following a bell-shaped profile that provides for the super-Gaussian reflectivity [84].

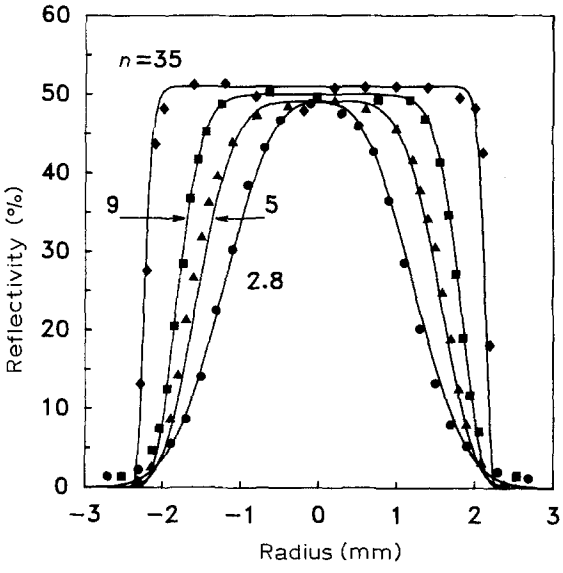

Figure 7 Intensity reflectivity profiles of four super-Gaussian mirrors (data points). The curves represent the best-fit super-Gaussian functions of order 2.8, 5, 9 and 35 and spot sizes 1.82, 1.92, 2.03 and 2.25 mm, respectively.

3.2 Unstable resonators with Gaussian mirrors

The earliest theoretical studies on VRM resonators were addressed to Gaussian unstable resonators, for which the eigenvalue diffraction equation leads to rigorous closed-form solutions for mode profiles and losses. Aperture-free resonators employing Gaussian mirrors were first analysed by solving the resonator integral equation for the electromagnetic field through asymptotic expansions [85]. Later, it was demonstrated that the modes of unstable resonators with Gaussian mirrors can be represented by Hermite–Gauss or Laguerre–Gauss functions [86]. A simple and elegant method to calculate the fundamental mode and the losses of Gaussian resonators is based on the ray matrix formalism as appropriate for Gaussian mirrors [87, 88]. This procedure relies on the resolution of the resonator self-consistency equation applied to the q-parameter which completely characterizes a Gaussian beam [89]. This approach is simpler than the manipulation of the diffraction integrals and allows general resonators, including also lens-like media, to be treated. The matrix formalism has also been extended to analyse higher order modes by means of the generalized Hermite–Gauss beams [90] or by means of mode expansions in Gaussian beams [91].

Using the matrix formalism, one finds that the mode of a resonator with a Gaussian mirror is a Gaussian beam, both for geometrically stable and for unstable resonators [88]. Accordingly, the magnification factor M^* is defined as

$$M^* = w_i/w_r \tag{25}$$

where w_i is the spot size of the Gaussian beam incident on the Gaussian mirror and w_r is the spot of the reflected beam [68]. For stable resonators the magnification M^* is generated mainly by diffraction, whereas for unstable resonators it is primarily due to the geometrical magnification M, defined according to the ray analysis [59]. It can be demonstrated that the two magnification factors are nearly equal under the hypothesis that [82, 92]

$$w_m/w_c \gg 2/(M-1)^{1/2} \tag{26}$$

where w_m is the Gaussian mirror spot size (see Equation 27) and $w_c = (\lambda L/\pi)^{1/2}$ is the mode spot size on the mirrors of a confocal stable resonator of the same length L. This inequality sets the condition for the validity of the geometrical optics approximation and is verified for all cases of practical interest, since unstable resonators are designed to have mode spot sizes much larger than those of confocal stable resonators. Within the validity of geometrical optics, Gaussian resonators can be considered to be a particular case of the wide class of super-Gaussian resonators, so we refer to the next section for the theoretical treatment.

So far we have considered aperture-free resonators. Actually, the active medium constitutes a sharp diaphragm which, without a proper resonator design, produces strong diffraction effects similar to those generated by the edge of the output mirror in traditional unstable resonators. As a consequence the advantages of using variable-reflectivity couplers are greatly reduced. In order to preserve a good beam quality, the mode amplitude at the rod edges should be only a small fraction of the peak amplitude. Theoretical and experimental investigations have shown that the intensity at the rod edges ought to be $< 13\%$ of the peak amplitude [75]. In order to satisfy the previous condition with the Gaussian function, the mode spot size inside the active material should be kept significantly narrower than the rod radius, so the overlap between the mode field and gain medium cross section is not optimized. To overcome this limitation we have proposed a new class of reflectivity profiles: the super-Gaussian functions, which provide a better filling of the rod cross section, as discussed in the next section.

3.3 Unstable resonators with super-Gaussian mirrors

The intensity reflectivity profile $R(r)$ of a super-Gaussian mirror is expressed by [81, 82]

$$R(r) = R_0 \exp\left[-2(r/w_m)^n\right] \tag{27}$$

where r is the radial coordinate, R_0 the peak reflectivity, w_m the mirror spot size and n the super-Gaussian order. This parameter determines the shape of the reflectivity from the Gaussian function ($n = 2$), up to the hard edge limit as n approaches infinity. The measured reflectivity profiles of four super-Gaussian mirrors, fabricated with the technique described in Section 3.1, are shown in Fig. 7 as data points. The full curves in the same figure are the best-fit super-Gaussian functions. For an unstable resonator with super-Gaussian mirrors the eigenvalue diffraction equation cannot be solved in a closed form. However, under the condition for the validity of the geometrical optics approach, the optical modes and losses can be calculated from the self-consistency equation [59, 66, 93]

$$\sigma u(r) = (1/M)\rho(r/M)\, u(r/M) \tag{28}$$

where $u(r)$ is the field amplitude of the beam incident on the mirror, $\rho(r) = [R(r)]^{1/2}$ is the amplitude reflectivity profile, the factor $1/M$ takes account of the amplitude due to the geometrical enlargement after a round trip and σ is the eigenvalue. For a generic reflectivity profile $\rho(r)$ the fundamental mode solution of Equation 28 can be expressed as an infinite product of the function $\rho(r)$ itself with scaled arguments [66]

$$u_0(r) = A \prod_{k=1}^{\infty} \rho(r/M^k)/\rho(0) \tag{29}$$

where A is an arbitrary amplitude factor. The higher order modes (u_m) are given by

$$u_m(r) = u_0(r) r^m \qquad m = 1, 2, \ldots \tag{30}$$

The eigenvalue for the generic mode of order m is

$$\sigma = \rho(0)\, M^{-(m+1)} \tag{31}$$

hence the round trip energy losses are given by

$$\gamma = 1 - \sigma^2 = 1 - R_0 M^{-2(m+1)} \tag{32}$$

For the case of a super-Gaussian resonator the product in Equation 29 converges to a super-Gaussian function of the same order as that of the reflectivity profile, so the fundamental mode on the output mirror can be expressed as [81]

$$u_0(r) = A \exp\left[-(r/w_i)^n\right] \tag{33}$$

where w_i is given by

$$w_i = w_m (M^n - 1)^{1/n} \tag{34}$$

Since, at least within the geometrical optics approximation, the fundamental mode resembles the reflectivity profile, a mirror of fairly high order forces an optical mode nearly squared that allows the requirement of low amplitude near to the rod edges to be met, while preserving a wide filling of the gain medium. For the lowest order mode the energy losses, according to Equation 32, reduce to

$$\gamma = 1 - R_0/M^2 \tag{35}$$

independently of the super-Gaussian order n. The mode intensity discrimination ratio, according to Equation 31, is given by $1/M^2$, which is significantly high even for moderate magnification factors M.

It is worth emphasizing that the above results hold only within the geometrical optics approximation, whose validity conditions need to be examined further. As is known, geometrical optics provides only for a very rough approximation for the modes of a traditional (hard-edge) unstable resonator, since the modes structure is determined mainly by the diffraction effects originating from the wavelets scattered at the edge of the output mirror [59]. The sharpness of the transition of the reflectivity from the top to the base, compared with the laser wavelength, is therefore the critical parameter to estimate the expected amount of diffraction effects [66]. For super-Gaussian mirrors the width of this transition region is related to the order n and to the spot size w_m. To compare the results of geometrical optics with those of diffractive optics, the cavity modes have been calculated numerically by means of the Huyghens–Fresnel diffraction integral in cylindrical coordinates, using the Prony method [94, 95], for several resonator configurations. A representative example of the comparison between diffractive and geometrical modes for the resonator shown in Fig. 8 with a super-Gaussian mirror of order $n = 9$ is given in Fig. 9. The agreement between the mode intensity profiles is quite good, even though a small ripple appears in the mode calculated by means of the diffraction theory. As expected, such a ripple vanishes for n around 2 and increases as the reflectivity profile approaches the hard edge limit. The diffractive mode profile of Fig. 9 has been calculated, assuming an infinitely large aperture of the active medium. For finite values of the rod diameter, some kind of irregularities are expected to be present, due to the mode perturbation at the rod edges. To simulate this effect by computer, a diaphragm has been introduced into the resonator model. Figure 10 shows the intensity of the beam incident on the super-Gaussian mirror of the resonator considered above with an internal diaphragm which cuts the geometrical

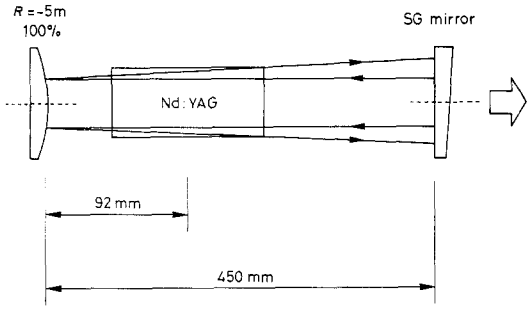

Figure 8 Schematic diagram of the unstable resonator configuration used by the authors for the experiments. The resonator is made by a flat super-Gaussian mirror and a 100% reflecting convex mirror of radius −5 m placed at 450 mm. The magnification is $M = 1.8$. The rod is 75 mm long with diameter 6.32 mm.

optics intensity distribution at about 5% of its peak value. Note that the coarse mode shape remains unchanged in spite of the diffraction effects, which produce fringes with high spatial frequency. Extensive calculations for various resonator configurations have demonstrated that the agreement becomes better when n is decreased and/or M is increased, and indicate that the results of geometrical optics are satisfactory provided that approximately $n < 15$, $M > 1.5$ and the cutting level is $< 5\%$.

3.3.1 Output beam profiles

The output beam transmitted through a super-Gaussian mirror is no longer super-Gaussian and presents a central dip if $R_0 M^n > 1$, as often occurs in cases of practical interest [82]. Therefore, the near-field presents a hollow whose depth and width increases with the order n. In the far-field, which represents the angular spectrum of the beam, the hollow results in side lobes which are fairly negligible for values of $n < 10$. As an example, the experimental near-field intensity profiles for the super-Gaussian resonators of Fig. 8 with mirrors or order 2.8, 9 and 35 are shown in Fig. 11a to c, compared with the theoretical beams calculated within the geometrical optics approximation and plotted in Fig. 11e to g. The shapes of the curves are in close agreement with the theoretical predictions. For all of the mirrors some rings are visible across the whole beam; this effect and, in particular, the central spike, arises from the diffraction wavelets due mainly to the rod aperture. The

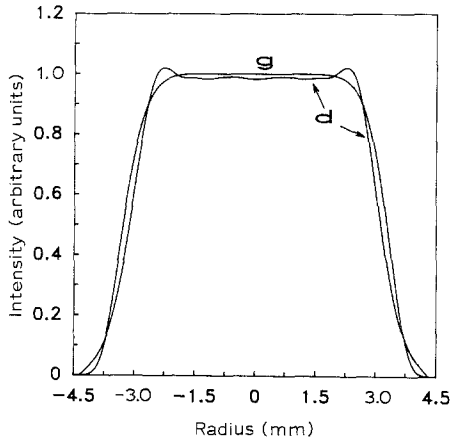

Figure 9 Comparison between mode-intensity profiles (beam incident on the output mirror) predicted by geometrical optics (g) and by diffraction theory (d) for the resonator shown in Fig. 8 with the super-Gaussian mirror of order $n = 9$. The rod diameter has been assumed to be infinite.

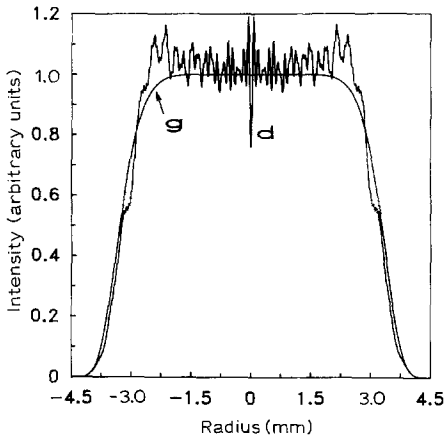

Figure 10 Mode intensity profile predicted by diffraction theory (d), for the same resonator as Fig. 9, when a 6.1 mm diameter aperture has been introduced inside the resonator model at 130 mm from the back mirror to take account of the effects of the rod aperture. The geometrical optics mode (g) is shown for comparison.

far-field patterns, recorded in the plane of minimum spot size of a converging lens, are shown in Fig. 12a to c. The related theoretical profiles, calculated by transforming the geometrical optics near-field profiles of Fig. 11 e to g, are plotted in Fig. 12 e to g. As n increases, side lobes begin to appear beside the central peak. The good agreement shown by measured far-field profiles and theoretically predicted patterns allow affirmation that, for all of the super-Gaussian resonators that have been tested, the beams are diffraction-limited. To confirm this observation further, we have compared the measured far-field profiles with the Fourier–Bessel transform of the experimental near-field profiles calculated assuming a plane phase front; an example of this comparison for the resonator with the mirror of order $n = 9$ is shown in Fig. 13. The agreement between the curves demonstrates that the assumption of constant phase for the near-field is substantially correct, and confirms that the beam is spatially coherent.

3.3.2 Output energy in free-running regime

To calculate the effect of the mode profile, and hence of the super-Gaussian order n, on the output energy, the influence of the transverse intensity profile on the gain saturation cannot be neglected. To this purpose the most precise method consists of solving the wave equations inside the resonator numerically, including the propagation in a saturating gain medium; these calculations require, however, a long computing time. To evaluate the energetic performances of lasers with super-Gaussian resonators as a function of the transverse mode profile easily, a simple theory, valid under widely satisfied approximations, has been developed [84]. The model relies on the laser rate equations that take account of the spatial variation of the gain saturation. A closed-form relationship for the output energy versus the pump energy with an explicit dependence on the mode profile has been derived. The input-output relationship obtained is valid for free-running pulsed lasers.

The space-dependent rate equations of a four-level laser are [96, 97]

$$\partial N/\partial t = W_p N_t - WN - N/\tau, \tag{36}$$

$$\mathrm{d}q/\mathrm{d}t = \int_{\mathrm{rod}} WN \,\mathrm{d}V - q/\tau_c \tag{37}$$

where N is the population inversion per unit volume, W_p the pump rate, N_t the concentration of active ions, W the stimulated emission rate, proportional to the mode intensity,

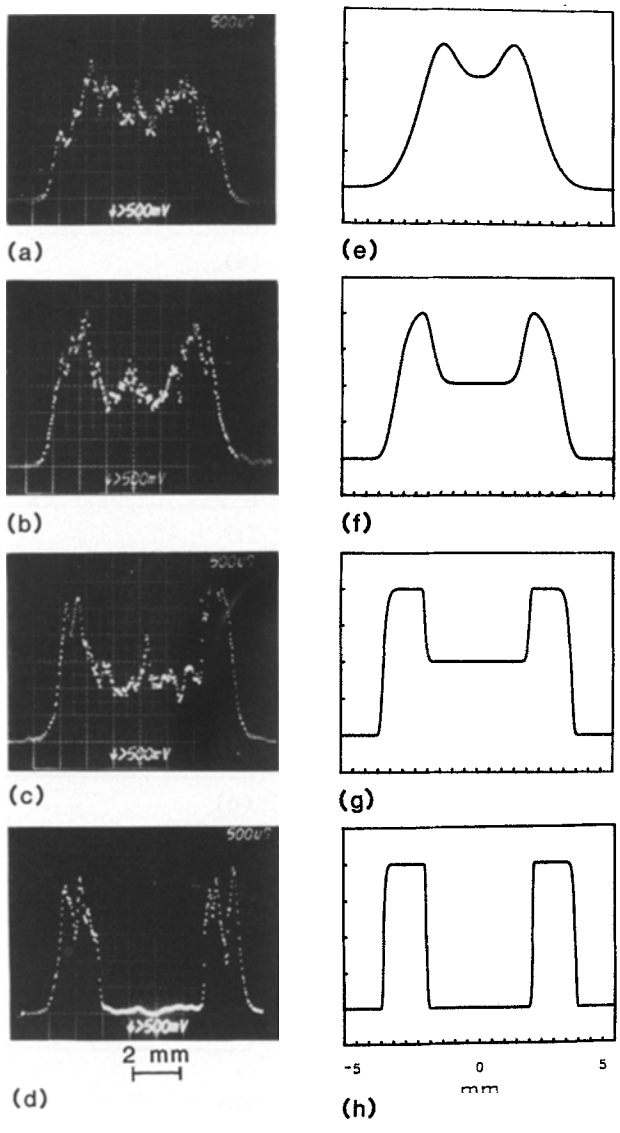

Figure 11 Experimental near-field profiles obtained by using the super-Gaussian mirrors or order (a) 2.8, (b) 9 and (c) 35 and (d) a hard-edge mirror with the resonator of Fig. 8. Plots e to h represent the corresponding geometrical optics modes.

τ the total lifetime of the upper laser level, q the number of photons inside the resonator, τ_c the photon lifetime and the integral in Equation 37 is extended over the rod volume.

Besides the general conditions for the validity of the rate equations approximation, we make the following hypotheses.

(a) The pump spatial distribution is uniform.

(b) The spontaneous decay term N/τ in Equation 36 is negligible because, in our case, the pump and the laser pulses are both shorter than the Neodymium upper laser level lifetime.

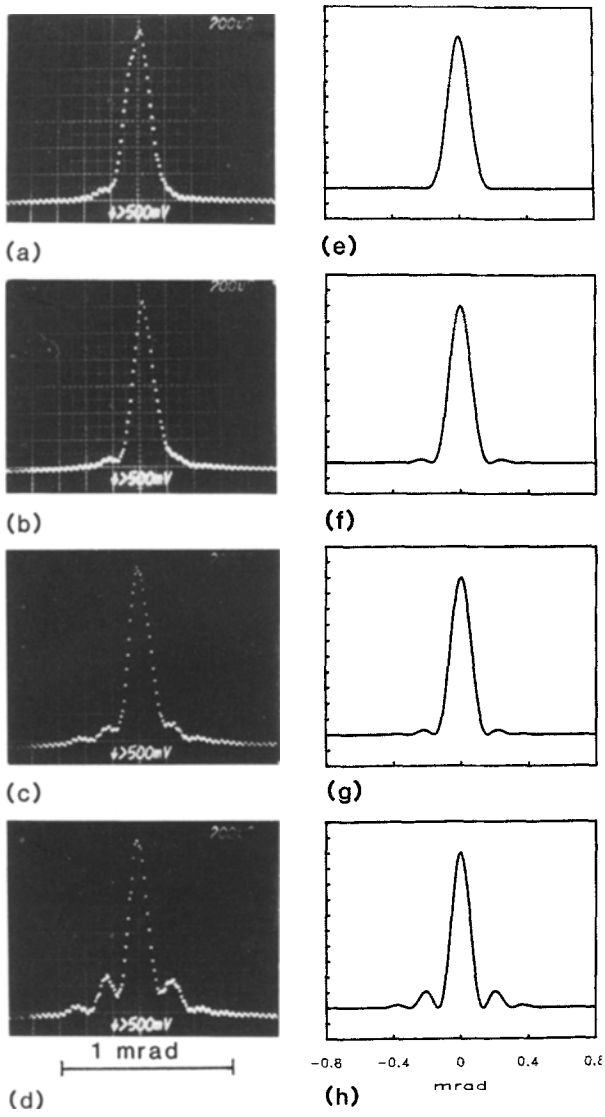

Figure 12 (a to d) Experimental far-field profiles corresponding to the near-field profiles of Fig. 11. Plots e to h represent the Fourier transform of the theoretical near-field profiles of Fig. 11.

(c) The energy emitted from the beginning of the pulse to any time t is proportional to the pump energy in excess of the threshold energy entering the laser up to the time t.

(d) The field intensity in the laser cavity is equal to the mode profile for the unloaded (without the rod) resonator, in spite of the effects of the saturable gain medium. This hypothesis is validated by the action of the super-Gaussian mirror, which strongly reshapes, at each round trip, the profile of the beam circulating inside the resonator.

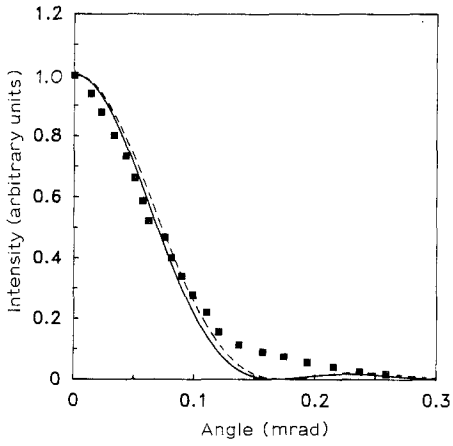

Figure 13 Comparison between the experimental far-field (■), the Fourier transform of the geometrical optics near-field (– – –) and the Fourier transform of the experimental near-field of Fig. 11b (——). The data refer to the resonator with the super-Gaussian mirror of order $n = 9$.

To solve Equations 36 and 37 we define the following three parameters:

$$\varepsilon = 2\sigma E_{out}/\gamma_1 h\nu \tag{38}$$

where σ is the emission cross section and γ_1 are the logarithmic losses of the output mirror;

$$\xi = N_0/N_c \tag{39}$$

which represents the normalized pump energy, N_0 being the inversion that would be present at the end of the pump pulse if the laser action were impeded and N_c the critical inversion; and

$$U(r) = |u(r)|^2 \tag{40}$$

which is the square of the mode amplitude of the unloaded resonator. According to assumption (d), $U(r)$ represents the transverse intensity profile in the laser cavity and is normalized over the rod cross section (S), so that

$$\int_S U(r)\, dS = 1 \tag{41}$$

Using the previous assumptions, after some lengthy algebra [84], we obtain the following expression for the output energy ($\propto \varepsilon$) as a function of the input energy ($\propto \xi$) and of the transverse mode profile, represented by $U(r)$:

$$\xi - 1 = \int_S \{\varepsilon U(r) - 1 + \exp[-\varepsilon U(r)]\}\, dS / \int_S \{\varepsilon U(r) - 1 + \exp[-\varepsilon U(r)]\}/\varepsilon U(r)\, dS \tag{42}$$

It is worth noting that this result is valid for any mode profile, not only for super-Gaussian profiles. This unusual input–output relationship reduces, for $U(r) =$ constant (corresponding to an ideally uniform intensity profile), to the much simpler form

$$\xi - 1 = \varepsilon/S \tag{43}$$

Hence, with the help of Equation 38, the output energy can be written explicitly as

$$E_{out} = (\gamma_1/2)(h\nu/\sigma)\, S(\xi - 1) \tag{44}$$

which is the linear input–output relationship obtained for c.w. lasers by the standard rate equation model.

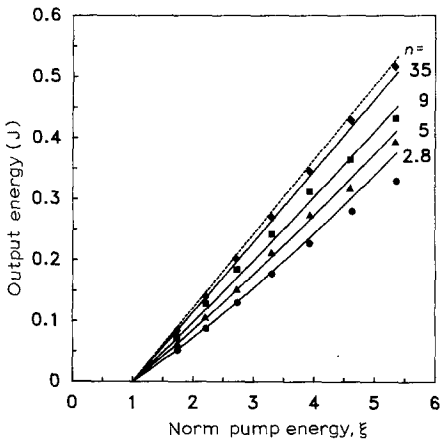

Figure 14 Theoretically predicted output energies versus pump energy normalized to the threshold energy for super-Gaussian resonator of Fig. 8 with mirrors of orders 2.8, 5, 9 and 35. The experimental energies obtained by the corresponding resonators are reported as data points. The broken curve refers to the energy calculated for a hypothetical resonator with a uniform mode.

Fig. 14 shows the output energies predicted by Equation 42 as a function of the normalized input energy for an Nd : YAG laser using the unstable resonator described in the previous section with mirrors of orders 2.8, 5, 9 and 35 (full curves). The output energies have been calculated assuming the mode profiles predicted by the geometrical optics. The broken curve, represents the plot of Equation 44 and shows the maximum energy that could ideally be extracted from the rod, with the given output losses, assuming a mode profile that completely fills the gain medium. In the same figure the experimental data have also been reported (data points). Since the peak reflectivity is 0.49 for all mirrors, the geometrical optics coupling losses are the same for all of the resonators (0.85) and the thresholds are theoretically identical. Experimentally, only minor differences around the value of 7.3 J have been detected. To fit the theoretical curves to the experimental data we have applied the least mean square algorithm with the neodymium cross section σ as a free parameter, because of the spread of data reported in the literature for this quantity. The best fit has been found for $\sigma = 4.6 \times 10^{-19}\,\mathrm{cm}^2$; this value appears to be acceptable, since it falls within the range of the reported data and, in particular, it agrees with some of them [98–100].

The curves show only minor deviation from straight lines and are in good agreement with the experimental data. From Fig. 14 it is apparent that, for a fixed pump energy, the output energy increases with n. However, the experimental trend and the theoretical calculations show that a resonator of super-Gaussian order $n > 10$ gives an output energy near to the theoretical maximum.

3.3.3 Comparative analysis

To appreciate fully the advantages offered by resonators using variable-reflectivity mirrors, the performances of such resonators ought to be compared with those of more-common configurations. Referring to Nd : YAG lasers, this comparison has been made for an unstable resonator using a parabolic mirror [80]. The output energy was comparable with the energy obtained from the same laser operated with a stable multimode resonator, whereas the beam quality was considerably improved by the single transverse mode oscillation provided by the VRM. A similar comparison has also been made for super-Gaussian resonators. The laser used for the measurement referred to in the previous section was equipped with a stable multimode resonator made by two concave mirrors of 8 m radius

curvature and reflectivity of 100 and 60%. Although at an input energy of 34 J the output energy (570 mJ) was 1.3 to 1.5 times greater than that of super-Gaussian resonators, the output beam was about 10 times the diffraction limit.

A more significant comparison refers to a traditional unstable resonator set up by replacing the output mirror of the super-Gaussian resonator of Fig. 8 with a hard-edge totally reflecting mirror. This mirror was made of an anti-reflection substrate with a central disc coated for high reflectivity. The diameter of the reflecting zone (4.4 mm) was chosen such that the mode intensity, calculated by geometrical optics, was tangent to the rod edge. Since $R_0 = 1$, the geometrical round trip losses were lower than those pertaining to the super-Gaussian resonators, and equal to 0.69. The experimental near- and far-field profiles obtained with such a resonator were shown in Fig. 11d and Fig. 12d and compared with the theoretical predictions (Figs 11 h and 12h). The near-field presents a central black hole due to the absence of the transmissive coupling by the output mirror, and the far-field is affected by remarkable side lobes. At the reference input energy of 34 J the output energy was 392 mJ, hence it was lower than that obtained from the most efficient super-Gaussian resonator ($n = 35$).

3.3.4 Q-switching

The high beam quality and the good energetic performances of unstable resonators with VRMs appear to be even more attractive in the Q-switching regime. In fact, this type of laser may find many important applications, such as in range finders, in laser radar and for harmonic generation.

A pulsed Nd:YAG laser with a resonator employing a parabolic mirror has been operated in the Q-switching regime and the output beam has been frequency-doubled [101]. In this case the conversion efficiency was as high as 60%. Active Q-switching has also been obtained with an Nd:YAG laser using a Gaussian unstable resonator [102]. The laser was operated in single longitudinal mode by means of the injection seeding technique, taking advantage of the single transverse mode oscillation provided by the Gaussian mirror.

The same super-Gaussian unstable resonator used in the free-running regime as described in Section 3.3.3 has also been tested in Q-switching, adding a Pokels cell and a Glan polarizer [103]. Figure 15 shows the Q-switching single-shot output energies obtained from the

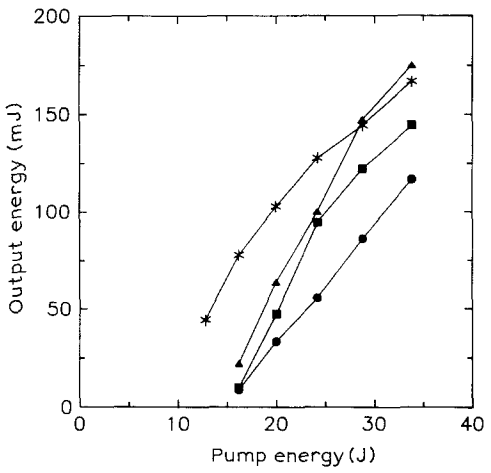

Figure 15 Output energy in Q-switching regime versus the electrical pump energy entering the lamp for three super-Gaussian resonators. The output energy from the same laser head with a stable multimode resonator is shown for comparison. (●) $n = 2.8$, (■) $n = 5$, (▲) $n = 9$ and (*) stable multimode.

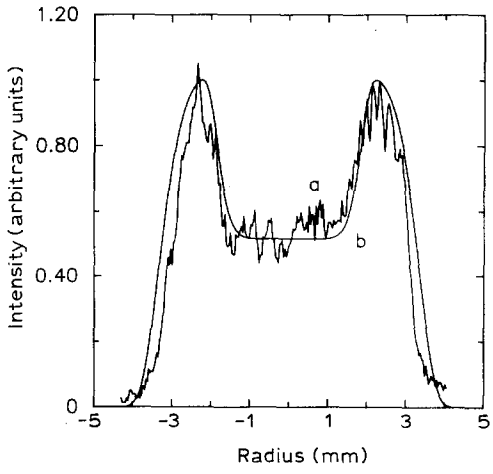

Figure 16 Near-field intensity profile obtained in Q-switching with the super-Gaussian mirror of order $n = 9$ (a), compared with the theoretical prediction (b).

laser. The near-field intensity profiles closely resemble the geometrical optics predictions, as can be seen as an example in Fig. 16, which refers to the super-Gaussian resonators of order $n = 9$. The high coherence degree of the output beams can be evaluated by means of Fig. 17, where the experimental far-field profile and the Fourier–Bessel transform of the experimental near-field profile are compared ($n = 9$).

3.3.5 Resonator design criteria

This section is devoted to summarizing simple guidelines, based on the experimental results, that can be applied to design super-Guassian resonators in such a way as to exploit the advantages of this configuration.

The mode spot size should be optimized for a good balancing between efficient filling of the gain medium and low beam perturbations caused by diffraction at the aperture of the active material. Equations 27, 34 and 35 allow the super-Gaussian mirror to be designed once the magnification M and the spot size w_i of the beam incident on the mirror are chosen. The choice of the geometrical magnification is somewhat arbitrary and depends strongly on the particular characteristic of the laser performances that one emphasizes. A trade-off has to be achieved among the mode intensity discrimination ratio ($1/M^2$), the output losses

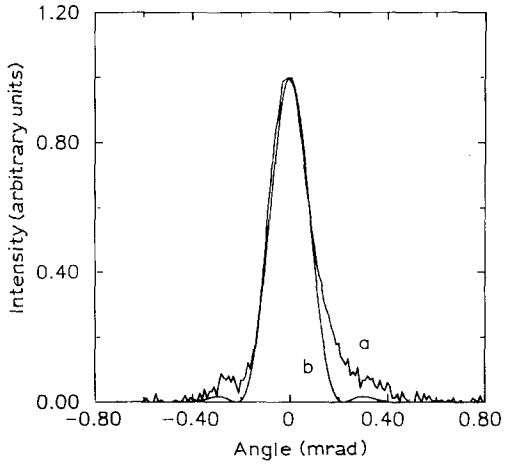

Figure 17 Far-field intensity profiles corresponding to the near-field of Fig. 16. (a) Measured profile and (b) Fourier–Bessel transform of the experimental near-field calculated assuming a plane phase front.

(see Equation 35) and the angular misalignment sensitivity. This last quantity, defined as the ratio of the angle by which the optical axis rotates and the tilting angle of the resonator mirror [104], is proportional to $M/(M-1)^2$. The choice of the peak reflectivity R_0 is not only related to the output losses, but also determines the shape of the output beam since the near-field profile is maximally flat if the additional constraint $R_0 M^n = 1$ is satisfied. Once the magnification and the peak reflectivity have been chosen, the mirror spot size can be calculated from Equation 34 if w_i is known. The spot size w_i can be optimized for a good balancing between efficient filling of the gain medium by the resonator mode and low beam perturbations caused by diffraction at the resonator apertures; this is achieved by choosing the cutting level of the mode intensity, due to the aperture, in the range 0.2 to 13% of the peak intensity [75, 84].

Finally the super-Gaussian order n of the mirror reflectivity profile has to be chosen. This is a critical design parameter, since it strongly influences the beam quality and the energetic performances of the laser system. The experimental results show that the values of the super-Gaussian order n of practical interest range from 5 to 10, with preference for the low values when the output beam uniformity has to be enhanced and preference for the high values when the maximum energetic efficiency has to be achieved.

4. Conclusions

We have presented a review of recent research activities in the field of optical resonators for diffraction-limited lasers of high power (or energy). In particular, two resonator configurations, which we have been developing in recent years, have been thoroughly treated, namely stable resonators for TEM_{00} operation with low-gain solid state lasers presenting strong thermal lensing effect in the active material and unstable resonators with radially variable-reflectivity mirrors of super-Gaussian profile for high-gain (solid state) lasers. In the case of stable resonators for c.w. solid state lasers, a general and comprehensive analysis of resonators with an internal focusing rod of variable power and arbitrary intracavity optical elements has shown that the concepts of dynamic stability, large mode volume, misalignment sensitivity and pump power stability range are crucial for a successful design. The main theoretical results, which have been experimentally confirmed by using an Nd : YAG laser, can be summarized as follows. First, any resonator presents as a function of the rod dioptric power two optically stable regions, which can be determined by straightforward equations. Secondly, the TEM_{00} mode volume is correlated through a fundamental relationship of inverse proportionality to the optical stability range of the resonator. Thirdly, the input pump power stability range depends only on the optomechanical properties of the laser medium. Finally, the criteria of minimum misalignment sensitivity of the resonator represent a key factor in the resonator design and discriminate among otherwise equivalent configurations in terms of TEM_{00} mode volume. On these bases, simple and readily applicable criteria for the design of large mode volume, dynamically stable resonators optimized for minimum misalignment sensitivity have been presented. The application of these design procedures to a c.w. Nd : YAG laser has led to a TEM_{00} output power of 18 W, which appears to be very close to the maximum obtainable with the rod size used in the experiments.

In the case of unstable resonators, which can be applied to high-gain lasers with large active material, such as pulsed solid state, CO_2 and excimers, the radially variable-reflectivity mirror are particularly useful in obtaining a superior beam quality. Although different devices with radially variable reflectivity profile have been developed, only those based on

mirrors with a dielectric layer of variable thickness have found significant practical applications. Among the various radially variable-reflectivity devices, the super-Gaussian dielectric mirrors present peculiar and very attractive advantages, as demonstrated by the detailed theoretical and experimental investigation we have reported: namely, the exploitation of the active medium is larger than that obtained with Gaussian reflectivity profile, providing for higher output energy; within the geometrical optics approximation (of quite general validity) the fundamental transverse mode of the resonator can be calculated algebraically and straightforward procedures for the analysis and the design of super-Gaussian resonators have been derived; and since the output power and the far-field brightness essentially depend on the super-Gaussian order, the tuning of this parameter allows for the choice of the most suitable mirror reflectivity profile in terms of output power and beam quality needed for each application. As for the output energy and extraction efficiency of super-Gaussian resonators, which strictly depend on both the mode profile and the gain dynamics, a theory that allows prediction in a close form of the energy extraction efficiency as a function of the shape of the reflectivity profile has been developed. The experiments performed on a flash-pumped Nd:YAG laser have shown the generation of diffraction-limited beams of energy comparable with that of stable multimode operation and even higher than that obtained with traditional unstable resonator configurations.

Acknowledgement

This present paper was partially supported by the National Research Council (CNR) of Italy, under the 'Progetto Finalizzato' on Electrooptics Technologies.

References

1. C. M. STICKLEY, *IEEE J. Quantum Electron.* **QE-2** (1966) 511.
2. L. M. OSTERINK and J. D. FOSTER, *Appl. Phys. Lett.* **12** (1968) 128.
3. F. A. LEVINE, *IEEE J. Quantum Electron.* **QE-7** (1971) 170.
4. L. M. PETERSON and D. C. CARMER, *ibid.* **QE-16** (1980) 650.
5. R. B. CHESLER and D. MAYDAN, *J. Appl. Phys.* **43** (1972) 2254.
6. J. STEFFEN, J. P. LÖRTSCHER and G. HERZIGER, *IEEE J. Quantum Electron.* **QE-8** (1972) 239.
7. J. P. LÖRTSCHER, J. STEFFEN and G. HERZIGER, *Opt. Quantum Electron.* **7** (1975) 505.
8. P. H. SARKIES, *Opt. Commun.* **31** (1979) 189.
9. D. C. HANNA, C. G. SAWYERS and M. A. YURATICH, *ibid.* **37** (1981) 359.
10. A. J. BERRY, D. C. HANNA and G. C. SAWYERS, *ibid.* **40** (1981) 54.
11. D. C. HANNA, C. G. SAWYERS and M. A. YURATICH, *Opt. Quantum Electron.* **13** (1981) 493.
12. S. DE SILVESTRI, P. LAPORTA and V. MAGNI, *Opt. Commun,* **57** (1986) 339.
13. A. P. DE FONZO, N. GITKIND, C. R. LUTZ and T. A. KUCHTA, *Appl. Opt.* **27** (1988) 3604.
14. R. IFFLÄNDER, H. P. KORTZ and H. WEBER, *Opt. Commun.* **29** (1979) 223.
15. H. P. KORTZ, R. IFFLÄNDER and H. WEBER, *Appl. Opt.* **20** (1981) 4124.
16. H. WEBER, R. M. IFFLÄNDER and P. SEILER, *SPIE Proc.* **650** (1986) 92.
17. K. P. DRIEDGER, R. M. IFFLÄNDER and H. WEBER, *IEEE J. Quantum Electron.* **QE-24** (1988) 665.
18. N. HODGSON, *SPIE Proc.* **1021** (1989) 89.
19. N. HODGSON and H. WEBER, *Opt. Quantum Electron.* **22** (1990) S39.
20. J. M. EGGLESTON, *IEEE J. Quantum Electron.* **QE-24** (1988) 1821.
21. V. MAGNI, *Appl. Opt.* **25** (1986) 107.
22. S. DE SILVESTRI, P. LAPORTA and V. MAGNI, *Opt. Commun.* **59** (1986) 43.
23. A. G. FOX and T. LI, *Proc. IEEE* **51** (1963) 80.
24. R. L. SANDERSON and W. STREIFER, *Appl. Opt.* **8** (1969) 2241.
25. J. A. ARNAUD, *ibid.* **8** (1969) 1909.
26. R. HAUCK, H. P. KORTZ and H. WEBER, *ibid.* **19** (1980) 6598.
27. S. DE SILVESTRI, P. LAPORTA and V. MAGNI, *Opt. Lett.* **11** (1986) 513.
28. *Idem, ibid.* **11** (1986) 785.

29. S. DE SILVESTRI, P. LAPORTA, V. MAGNI and O. SVELTO, *SPIE Proc.* **701** (1987) 118.
30. D. METCALF, P. DE GIOVANNI, J. ZACHOROWSKI and M. LEDUC, *Appl. Opt.* **26** (1987) 4508.
31. V. MANGI, *J. Opt. Soc. Am.* **A4** (1987) 1962.
32. S. DE SILVESTRI, P. LAPORTA and V. MAGNI, *Opt. Commun.* **65** (1988) 373.
33. *Idem, IEEE J. Quantum Electron.* **QE-23** (1987) 1999.
34. H. VANHERZEELE, *Appl. Opt.* **27** (1988) 3608.
35. *Idem, Opt. Lett.* **13** (1988) 369.
36. E. REED and G. FRANGINEAS, *SPIE Proc.* **1223** (1990) 247.
37. J. D. FOSTER and L. M. OSTERINK, *J. Appl. Phys.* **41** (1970) 3656.
38. W. KOECHNER, *Appl. Opt.* **9** (1970) 1429.
39. *Idem, ibid.* **9** (1970) 2548.
40. T. KIMURA and K. OTSUKA, *IEEE J. Quantum Electron.* **QE-7** (1971) 403.
41. W. KOECHNER, in 'Solid State Laser Engineering', 2nd Edn (Springer-Verlag, Berlin, 1988) p. 357.
42. H. KOGELNIK, *Bell Syst. Tech. J.* **44** (1965) 455.
43. A. E. SIEGMAN, in 'Lasers' (Oxford University Press, Oxford, 1986) p. 616.
44. A. GERRARD and J. M. BURCH, in 'Introduction to Matrix Methods in Optics' (Wiley, London, 1975) pp. 106, 286.
45. J. A. ARNAUD, in 'Beam and Fiber Optics' (Academic Press, New York, 1976) Ch. 4.
46. M. NAZARATHY, A. HARDY and J. SHAMIR, *J. Opt. Soc. Am.* **A3** (1986) 1360.
47. A. E. SIEGMAN, in 'Lasers' (Oxford University Press, Oxford, 1986) p. 607.
48. P. BAUES, *Opto-Electronics* **1** (1969) 37.
49. A. E. SIEGMAN, in 'Lasers' (Oxford University Press, Oxford, 1986) p. 815.
50. S. DE SILVESTRI, P. LAPORTA and V. MAGNI, in 'Proceedings of Lasers '85' (STS Press, McLean, Virginia, 1986) p. 616.
51. J. DEMBOWSKY and H. WEBER, *Opt. Commun.* **42** (1982) 133.
52. W. KOECHNER, in 'Solid State Laser Engineering', 2nd Edn (Springer-Verlag, Berlin, 1988) p. 361.
53. E. REED, *IEEE J. Quantum Electron.* **QE-21** (1985) 1625.
54. J. Y. LIU, K. C. LIU and M. G. COHEN, in 'Technical Digest of CLEO, '86' (Optical Society of America, Washington, DC, 1986) p. 108.
55. H. VANHERZEELE, *Appl. Opt.* **28** (1989) 4042.
56. T. CHIN, R. C. MORRIS, O. KAFRI, M. LONG and D. F. HELLER, *Proc. Soc. Photon. Instrum. Engng.* **622** (1986) 53.
57. H. KOGELNIK and T. LI, *Appl. Opt.* **5** (1966) 1550.
58. M. SAEED, D. KIM and L. F. DI MAURO, *Appl. Opt.* **29** (1990) 1752.
59. A. E. SIEGMAN and R. ARRATHOON, *IEEE J. Quantum Electron.* **QE-3** (1967) 156.
60. A. E. SIEGMAN, in 'Lasers' (Oxford University Press, Oxford, 1986) p. 874.
61. P. G. GOBBI and G. C. REALI, *Opt. Commun.* **52** (1984) 195.
62. P. G. GOBBI, S. MOROSI, G. C. REALI and A. S. ZARKASI, *Appl. Opt.* **24** (1985) 26.
63. C. JIANWEN, A. LUCHES, V. NASSISI and M. R. PERRONE, *J. Modern Opt.* **37** (1990) 75.
64. K. YASUI, M. TANAKA and S. YAGI, *J. Appl. Phys.* **65** (1989) 17.
65. K. YASUI, S. YAGI and M. TANAKA, *Appl. Opt.* **29** (1990) 1277.
66. Y. A. ANAN'EV and V. E. SHERSTOBITOV, *Soviet J. Quantum Electron.* **1** (1971) 263.
67. G. GIULIANI, Y. K. PARK and R. L. BYER, *Opt. Lett.* **5** (1980) 491.
68. J. M. EGGLESTON, G. GIULIANI and R. L. BYER, *J. Opt. Soc. Am.* **71** (1981) 1264.
69. D. J. HARTER and J. C. WALLING, *Opt. Lett.* **11** (1986) 706.
70. E. ARMANDILLO and G. GIULIANI, *ibid.* **10** (1985) 445.
71. S. DE SILVESTRI, P. LAPORTA and V. MAGNI, *J. Opt. Soc. Am.* **A4** (1987) 1413.
72. S. DE SILVESTRI, P. LAPORTA, V. MAGNI and O. SVELTO, *Opt. Lett.* **12** (1987) 84.
73. P. LAVIGNE, N. McCARTHY and J. G. DEMERS, *Appl. Opt.* **24** (1985) 2581.
74. N. McCARTHY and P. LAVIGNE, *Opt. Lett.* **10** (1985) 553.
75. A. PARENT, N. McCARTHY and P. LAVIGNE, *IEEE J. Quantum Electron.* **QE-23** (1987) 222.
76. D. V. WILLETTS and M. R. HARRIS, *ibid.* **QE-24** (1988) 849.
77. P. LAVIGNE, A. PARENT, D. PASCALE and N. McCARTHY, *ibid.* **QE-22** (1986) 2200.
78. C. ZIZZO, C. ARNONE, C. CALI' and S. SCIORTINO, *Opt. Lett.* **13** (1988) 342.
79. S. DE SILVESTRI, P. LAPORTA, V. MAGNI, O. SVELTO, C. ARNONE, C. CALI', S. SCIORTINO and C. ZIZZO, *Opt. Commun.* **67** (1988) 229.

80. K. J. SNELL, N. McCARTHY, M. PICHE and P. LAVIGNE, *ibid.* **65** (1988) 377.
81. S. DE SILVESTRI, P. LAPORTA, V. MAGNI and O. SVELTO, *IEEE J. Quantum Electron.* **QE-24** (1988) 1172.
82. S. DE SILVESTRI, P. LAPORTA, V. MAGNI, O. SVELTO and B. MAJOCCHI, *Opt. Lett.* **13** (1988) 201.
83. G. EMILIANI, A. PIEGARI, S. DE SILVESTRI, P. LAPORTA and V. MAGNI, *Appl. Opt.* **28** (1989) 2832.
84. S. DE SILVESTRI, V. MAGNI, O. SVELTO and G. VALENTINI, *IEEE J. Quantum Electron.* **QE-26** (1990) 1500.
85. N. G. VAKHIMOV, *Radio Engng. Electron. Phys.* **10** (1965) 1439.
86. H. ZUCKER, *Bell Syst. Tech. J.* **49** (1970) 2349.
87. L. W. CASPERSON and S. D. LUNNAM, *Appl. Opt.* **14** (1975) 1193.
88. A. YARIV and P. YEH, *Opt. Commun.* **13** (1975) 370.
89. A. E. SIEGMAN, in 'Lasers' (Oxford University Press, Oxford, 1986) p. 663.
90. D. M. WALSH and L. V. KNIGHT, *Appl. Opt.* **25** (1986) 2947.
91. U. GANIEL and A. HARDY, *ibid.* **15** (1976) 2145.
92. A. E. SIEGMAN, in 'Lasers' (Oxford University Press, Oxford, 1986) p. 913.
93. V. E. SHERSTOBITOV and G. N. VINOKUROV, *Soviet J. Quantum Electron.* **2** (1972) 224.
94. A. E. SIEGMAN and H. Y. MILLER, *Appl. Opt.* **9** (1970) 2729.
95. W. D. MURPHY and M. L. BERNABE, *ibid.* **17** (1978) 2358.
96. O. SVELTO, in 'Principles of Lasers', 3rd Edn (Plenum Press, New York, 1989) p. 465.
97. T. Y. FAN and R. L. BYER, *IEEE J. Quantum Electron.* **QE-23** (1987) 605.
98. M. BIRNBAUM, A. W. TUCKER and C. L. FINCHER, *J. Appl. Phys.* **52** (1981) 1212.
99. K. FUHRMANN, N. HODGSON, F. HOLLINGER and H. WEBER, *ibid.* **62** (1987) 4041.
100. M. D. SHINN, F. P. MILANOVICH and J. N. ROE, in 'Technical Digest CLEO '89' (Optical Society of America, Washington, DC, 1989) p. 242.
101. A. PARENT and P. LAVIGNE, *Opt. Lett.* **14** (1989) 399.
102. A. CAPRARA, S. BUTCHER and R. AUBERT, *SPIE Proc.* **912** (1988) 20.
103. S. DE SILVESTRI, V. MAGNI, S. TACCHEO and G. VALENTINI, *Opt. Lett.* **16** (1991) 642.
104. W. F. KRUPKE and W. R. SOOY, *IEEE J. Quantum Electron.* **QE-5** (1969) 575.